Chinese Journal of
POLYMER SCIENCE

RESEARCH ARTICLE

https://doi.org/10.1007/s10118-026-3803-6
Chinese J. Polym. Sci.

Highly Expanded Open-cell Poly(vinylidene fluoride) Foams Achieved by Microcellular Foaming for Efficient Oil Adsorption and Thermal Insulation

Chao Wei[a,b], Jia-Long Chai[a,b], Lei Zhang[a,b], Zhao-Rui Xu[a,b*], and Gui-Long Wang[a,b,c*]

[a] *State Key Laboratory of Advanced Equipment and Technology for Metal Forming, Shandong University, Jinan 250061, China*
[b] *Key Laboratory for Liquid-Solid Structural Evolution and Processing of Materials (Ministry of Education), Shandong University, Jinan 250061, China*
[c] *Linyi Huafeng Seal Technology Co., Ltd., Linyi 276628, China*

Abstract Environmental protection and management are crucial to sustainable development. Microcellular polymer foams with open-cell structures have attracted significant attention for applications in oil-spill remediation and thermal management owing to their low density, large specific surface area, high adsorption capacity, and superior thermal insulation. Poly(vinylidene fluoride) (PVDF) is a promising candidate material because of its high durability, hydrophobicity, flame retardancy, and environmental resistance. However, the preparation of high-performance PVDF foams with open-cell structures is limited by their insufficient melt strength following crystal melting and narrow melting window. In this study, a green and efficient microcellular foaming strategy based on molten-crystalline transient regulation was employed to fabricate PVDF foams with high expansion ratios and highly open-cell structures. This strategy enables the precise regulation of the PVDF melt strength across an extended crystallization temperature range, thereby achieving excellent foamability. The resulting PVDF foams exhibited a high expansion ratio of 33.4, a significantly broadened foaming window of 120–160 °C, and a maximum open-cell content of 94.7%. These foams demonstrate outstanding comprehensive properties, including a low thermal conductivity of 31.26 $mW \cdot m^{-1} \cdot K^{-1}$, high oil adsorption capacities ranging from 13.7 $g \cdot g^{-1}$ to 28.0 $g \cdot g^{-1}$, as well as good cyclic adsorption stability and compression performance. This work provides a green and efficient strategy for constructing high-performance open-cell PVDF foams, demonstrating promising potential for broad applications, such as oil-spill cleanup and thermal insulation.

Keywords Microcellular polymer foam; Poly(vinylidene fluoride); High expansion ratio; Open-cell structure; Oil adsorption

Citation: Wei, C.; Chai, J. L.; Zhang, L.; Xu, Z. R.; Wang, G. L. Highly expanded open-cell poly(vinylidene fluoride) foams achieved by microcellular foaming for efficient oil adsorption and thermal insulation. *Chinese J. Polym. Sci.* https://doi.org/10.1007/s10118-026-3803-6

INTRODUCTION

The advancement of modern industries coupled with growing environmental and climate concerns has intensified the demand for green and sustainable technologies.[1–3] Significant challenges to energy conservation and environmental protection arise from oil spills, waste oil discharge, inefficient thermal management, *etc*.[4–6] Oil-water separation is a key technology for treating oil spills and oily wastewater, and physical adsorption using oil-adsorbing materials is an important method for achieving efficient oil-water separation. High-performance oil-adsorbing materials, such as foams, aerogels, fibers, nonwovens, membranes, and felts, should possess excellent oleophilicity and hydrophobicity, low density, high porosity, and a highly open-cell structure.[7] Among these, microcellular polymer foams with open-cell structures exhibit broad application prospects in oil adsorption and thermal management, owing to their outstanding processability, low density, good corrosion resistance, excellent adsorption capacity, and superior thermal insulation properties.[8,9]

Constructing microcellular polymer foams with high porosity and interconnected open-cell structures can effectively reduce the thermal conductivity and enhance the oil adsorption capacity, thereby offering potential solutions to the aforementioned challenges. Among the various fabrication methods, including phase separation[10,11], polymerization[12,13], chemical foaming[14], and chemical vapor deposition[15], the microcellular foaming technique with supercritical carbon dioxide ($scCO_2$) is widely recognized as an effective and environmentally friendly approach for producing microcellular polymer foams with open-cell structure[16–18]. Carbon dioxide has become one of the most commonly used green foaming media in the field of polymer microcellular foaming, owing to its unique physicochemical properties.[19] It combines the high diffusion coefficient of a gas with the high solvation power of a liquid, offering advantages such as non-toxicity, non-flammability, recyclability, and no residual

* Corresponding authors, E-mail: xuzhaorui@mail.sdu.edu.cn (Z.R.X.)
E-mail: guilong@sdu.edu.cn (G.L.W.)
Received May 15, 2026; Accepted July 3, 2026; Published online September 10, 2026

contamination, meeting the requirements of green manufacturing and sustainable development. In the foaming process, cell wall rupture is considered the main pathway for the formation of open-cell structures.[20,21] When the local stress exceeds the limit that the polymer melt can withstand, the cell wall ruptures and forms interconnected channels. A lower melt strength facilitates cell coalescence and open-cell formation, but an excessively low melt strength can lead to cell collapse. Therefore, achieving a balance between cell stability and open-cell formation is key to the preparation of foams with high open-cell content.[22,23]

Poly(vinylidene fluoride) (PVDF), a thermoplastic fluoropolymer, exhibits not only excellent processability, but also outstanding comprehensive properties, including chemical resistance, high thermal stability, weatherability, and inherent flame retardancy.[24,25] These advantages endow microcellular PVDF foams with significant application potential in insulation, flame-retardant components, and adsorption systems, while also granting them long-term service capabilities in harsh environments.[26,27] However, PVDF exhibits pronounced crystallization behavior characterized by high crystallinity, narrow melting window, rapid crystallization kinetics, and poor melt strength after melting.[28–30] Such crystallization behavior poses major challenges for conventional heating-mediated foaming process, which relies on temperature increases to control the PVDF melt strength.

The traditional view holds that increased crystallinity restricts chain mobility and reduces gas diffusion capacity, thereby inhibiting cell growth, often leading to non-uniform cell structures or low expansion ratios.[31] However, an increasing number of recent studies have shown that a moderate crystalline structure can significantly enhance the melt strength, providing support for stable cell growth.[32–34] Therefore, crystallization exerts a dual effect on foaming behavior: on the one hand, it hinders gas diffusion and cell expansion; on the other hand, it enhances melt stability and suppresses cell collapse. To this end, various strategies are employed to regulate the crystallization behavior of polymers, including temperature control, pressure control, gas-induced crystallization, strain-induced crystallization, *etc*. Among them, the utilization of the foaming agent $scCO_2$ profoundly affects the crystallization behavior of semi-crystalline polymers.[35–37] Hence, the utilization of CO_2 to regulate the coupling relationship between the polymer crystalline structure and foaming behavior has become an important research direction in microcellular foaming.

Compared with conventional heating-mediated foaming, the molten-crystalline transient regulation foaming strategy exhibits significant advantages in controlling crystallization behavior when fabricating semi-crystalline polymer foams.[38–40] This strategy utilizes the gradual increase in melt strength during the molten-crystalline transition of the polymer, thereby triggering foaming at a specific crystallization stage and enabling the polymer melt to simultaneously possess a high gas content and appropriate strength. The plasticizing effect of $scCO_2$ increases the mobility of the molecular chains and raises the supercooling requirement for chain crystallization. This lowers the crystallization onset temperature, broadens the crystallization temperature window, and prolongs the molten-crystalline transition process within the PVDF melt. Consequently, the melt strength, strongly influenced by the crystallization behavior, can be effectively tuned over a wider temperature range, enabling precise control over foaming. Moreover, crystallization-induced stress concentration is recognized as an effective mechanism for promoting open-cell formation. During foaming, the incompletely crystallized chains undergo further crystallization under strain-induced hardening. The resulting crystals, which possess a modulus mismatch with the surrounding amorphous phase, create stress concentration points, promote cell wall rupture, and form a unique interconnected open-cell structure. Collectively, these features render the molten-crystalline transient regulation strategy an efficient and promising approach for fabricating semi-crystalline polymer foams with light weight and high open-cell content.

In this study, a green and efficient microcellular foaming strategy based on molten-crystalline transient regulation was employed to fabricate highly open-cell PVDF foams for oil adsorption and thermal insulation applications. The thermal behavior and melt strength evolution of PVDF were first investigated using rheological analysis and differential scanning calorimetry (DSC). By optimizing the foaming conditions, PVDF foams with an expansion ratio of 33.4 and an open-cell content of 94.7% were successfully obtained. The resulting foams exhibit excellent comprehensive performance, including high oil adsorption capacities of 13.7–28.0 $g \cdot g^{-1}$, good cyclic adsorption stability over ten adsorption-desorption cycles, and favorable mechanical robustness. Additionally, the PVDF foams demonstrate outstanding thermal insulation performance, with a low thermal conductivity of 31.26 $mW \cdot m^{-1} \cdot K^{-1}$. This study provides a simple and environmentally friendly strategy for constructing high-performance open-cell PVDF foams and highlights their potential for applications in oil-spill remediation and thermal management.

EXPERIMENTAL

Materials

Commercial poly(vinylidene fluoride) (PVDF), Kynar® 720, with a density of 1.78 $g \cdot cm^{-3}$ and molecular weight of approximately 150 kDa, was purchased from Arkema Inc., France. Carbon dioxide (CO_2) with a purity of 99.9%, used as foaming agent, was supplied by Deyang Gas Company, China.

Foaming Sample Preparation

Batch foaming experiments were performed in a self-developed high-pressure autoclave equipped with a PID temperature control system and a high-pressure plunger pump (260D, TELEDYNE ISCO, USA). The schematic diagram of the equipment used for the microcellular foaming experiment is shown in Fig. 1. When the solid PVDF was heated to 190 °C in the autoclave, a 20-min saturation process was conducted under a certain CO_2 pressure to establish a homogeneous PVDF/CO_2 system. Next, the autoclave was cooled to the desired foaming temperature at a rate of 10 $°C \cdot min^{-1}$, followed by rapid depressurization to trigger foaming. Finally, the resulting foams were immediately quenched in ice water to stabilize their cellular structure. The saturation pressures in foaming experiments were 13.8, 20.7 and 27.6 MPa, and the foaming temperatures were 120, 130, 140, 150 and 160 °C.

https://doi.org/10.1007/s10118-026-3803-6

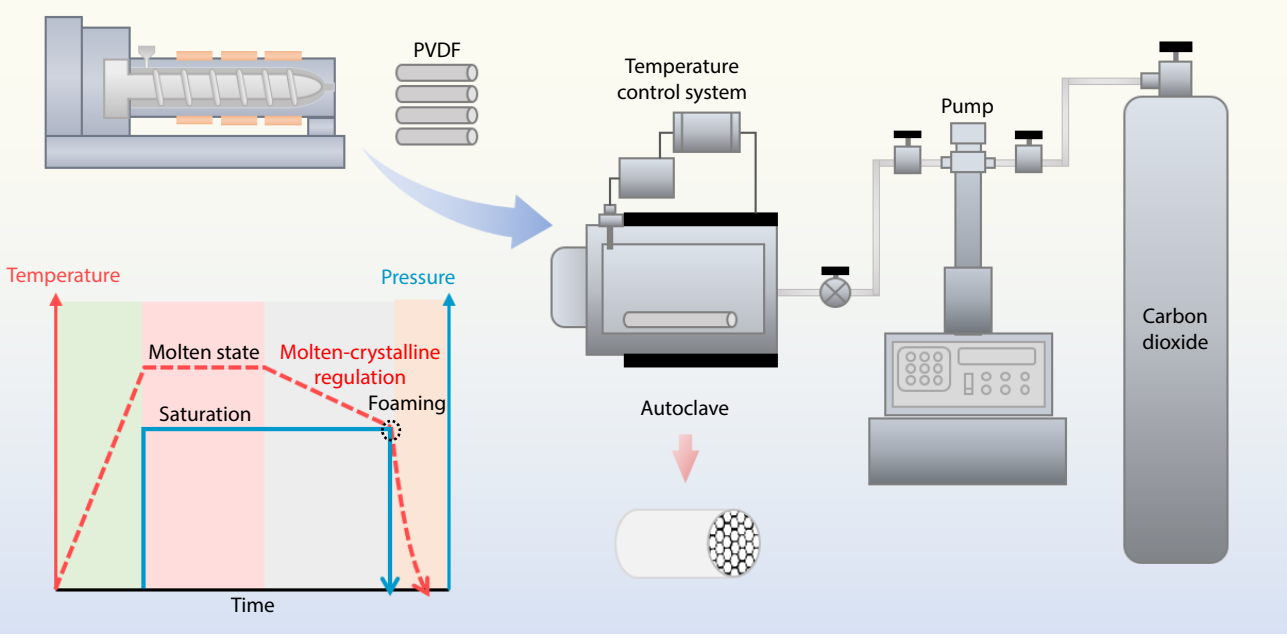

Fig. 1 The schematic diagram of microcellular foaming strategy based on molten-crystalline transient regulation.

Characterization

Rheological measurements

The rheological behavior of solid PVDF was evaluated using a rotational rheometer (Mars 40, Thermo Fisher Scientific, USA) with a 20 mm parallel disk and a 1.0 mm gap. Temperature sweep measurements were conducted during cooling from 200 °C to 100 °C at a cooling rate of 3 °C·min^{-1}, with a strain amplitude of 1.0% and an angular frequency of 1 rad·s^{-1}. The crystallization behavior of solid PVDF was characterized using a differential scanning calorimeter (DSC 400, NETZSCH, Germany). A sample of approximately 10 mg was sealed in an aluminum crucible and heated to 200 °C at a heating rate of 20 °C·min^{-1}, followed by an isothermal treatment at 200 °C for 5 min to eliminate thermal history. Then, the sample was cooled to 30 °C at a cooling rate of 10 °C·min^{-1}.

Morphology characterization

The expansion ratio (ϕ) of the PVDF foams was measured according to the water displacement method, using the following equation:

$$\phi = \frac{\rho_s}{\rho_f} \tag{1}$$

where ρ_s and ρ_f are the densities of the solid PVDF and PVDF foam, respectively. The cellular morphology of the PVDF foams was examined by scanning electron microscopy (SEM, SEM-30 Plus, COXEM Co., Ltd., Korea). The specimens were cryo-fractured rapidly after immersion in liquid nitrogen for 20 min. The fracture surfaces were sputter-coated using a sputter coater (ETD-900M, Elaborate Technology Development, China) to avoid electron charging prior to the SEM observation. Cell size and cell density were quantified using commercial software (Nano Measure) according to the SEM images. At least 200 cells were counted for each sample to ensure statistical reliability. The cell density (N_0) was calculated as follows:

$$N_0 = \phi\left(\frac{n}{A}\right)^{3/2} \tag{2}$$

where n is the number of cells within the selected area A.

Open-cell content measurement

The true volumes of the PVDF foams were measured using a gas pycnometer (AccuPyc II 1340, Micromeritics, USA) with helium as the displacement gas. The open-cell content (OC) was calculated as:

$$\text{OC}\ (\%) = \frac{V_{open}}{V_{total}} \times 100 = \left(1 - \frac{V_{true}}{V_{total}}\right) \times 100 \tag{3}$$

where V_{total} is the apparent bulk volume of the foam, V_{true} is the gas-impenetrable volume measured by helium pycnometry, including the polymer matrix and closed-cell volume, and V_{open} is the helium-accessible open-cell volume. For each foaming condition, five specimens were tested and the average values with the corresponding errors were recorded.

Water contact angle measurement

The water contact angle was measured using a contact angle goniometer (JC2000D, Powereach, China) with deionized water. The measurements were performed at three different positions, and the average values were recorded.

Oil adsorption property

The oil adsorption properties of the PVDF foams were evaluated using carbon tetrachloride (CCl_4), cyclohexane, ethyl acetate, diesel fuel, silicone oil and peanut oil. After removing the surface skin, a cubic PVDF foam with a length of 8 mm was weighed (m_0) and then immersed in the oils. After a predefined time, the sample was removed and the surface oil was rapidly wiped off. Then, the mass of the oil-laden PVDF foam (m_1) was recorded. The oil adsorption capacity (Q_e) was calculated as follows:

$$Q_e = \frac{m_1 - m_0}{m_0} \tag{4}$$

The cyclic oil adsorption property was assessed by the desorption of CCl_4 from the foam *via* evaporation at room temperature and atmospheric pressure after reaching adsorption

https://doi.org/10.1007/s10118-026-3803-6

equilibrium. This process was repeated 10 times, and the corresponding capacities were recorded.

Compression performance

The compression performance of the PVDF foam was studied using a universal testing machine (HDW-2000, Hengxu, China). The PVDF foams were cut into cubes with lengths of 10 mm. The maximum strain and strain loading rate were set to 60% and 1.0 mm·min^{-1}, respectively.

Thermal insulation characterization

The thermal conductivities of the solid PVDF and PVDF foams were measured using a thermal constant analyzer (TPS 2500S, Hot Disk, Sweden) based on the transient plane source method. Two identical specimens with flat, skin-free surfaces had dimensions of 10 mm × 10 mm × 10 mm. Infrared thermal images were recorded using an IR camera (E86, Flir, USA). The samples were placed tightly on a hot plate maintained at 80 °C. After 5 min, the temperature on the upper surface of the PVDF specimens stabilized, indicating that thermal equilibrium had been reached. Then, the results were recorded. The samples were arranged with adequate spacing to prevent interactions between them. The entire test was conducted at the room temperature of 23 °C.

RESULTS AND DISCUSSION

Rheological and Thermal Behaviors during Cooling

The PVDF melt undergoes complex molecular dynamics evolution accompanied by a melt-crystallization transition during the cooling process, which is highly temperature-dependent. Rheological characterization provides critical insights into the sensitivity of the melt strength, thereby offering a fundamental basis for the design of foaming processes. As shown in Figs. 2(a)–2(c), the storage modulus (G'), loss modulus (G''), and complex viscosity (η^*) of the PVDF melt exhibit similar trends with decreasing temperature. Specifically, these parameters increased gradually as the temperature decreased from 200 °C to approximately 148 °C, followed by a sharp increase below about 148 °C. The gradual increase in the viscosity and moduli can be attributed to the reduced thermal motion and decreased segmental mobility of the polymer chains at lower temperatures. The subsequent sharp increase is mainly associated with the crystallization behavior of PVDF. As illustrated in Fig. 2(d), the DSC cooling curve indicates that PVDF completes crystallization within the temperature range of approximately 130–141 °C during cooling, whereas the melting process during heating occurs between approximately 163–178 °C. These results are consistent with the abrupt changes observed in rheological properties. The crystals act as rigid physical crosslinking points and obstacles to molecular motion in polymers, significantly enhancing the stiffness while severely restricting chain slippage and flow.[41]

Crystallization behavior plays a crucial role in determining the foamability of PVDF. Hence, precise regulation of the molten-crystalline transient state is essential for achieving its optimal foamability. In heating-mediated foaming processes, PVDF contains a large number of well-developed crystals and interconnected crystalline regions below the onset melting temperature, corresponding to high relative crystallinity, as shown in Fig. 2(e). Upon further heating, the relative crystallinity rapidly approaches zero. The relative crystallinity fluctuated too rapidly over short periods, making it difficult to precisely control the melt strength of PVDF to an optimal level. This limitation hinders PVDF from achieving its full foaming potential. In contrast, under the molten-crystalline tran-

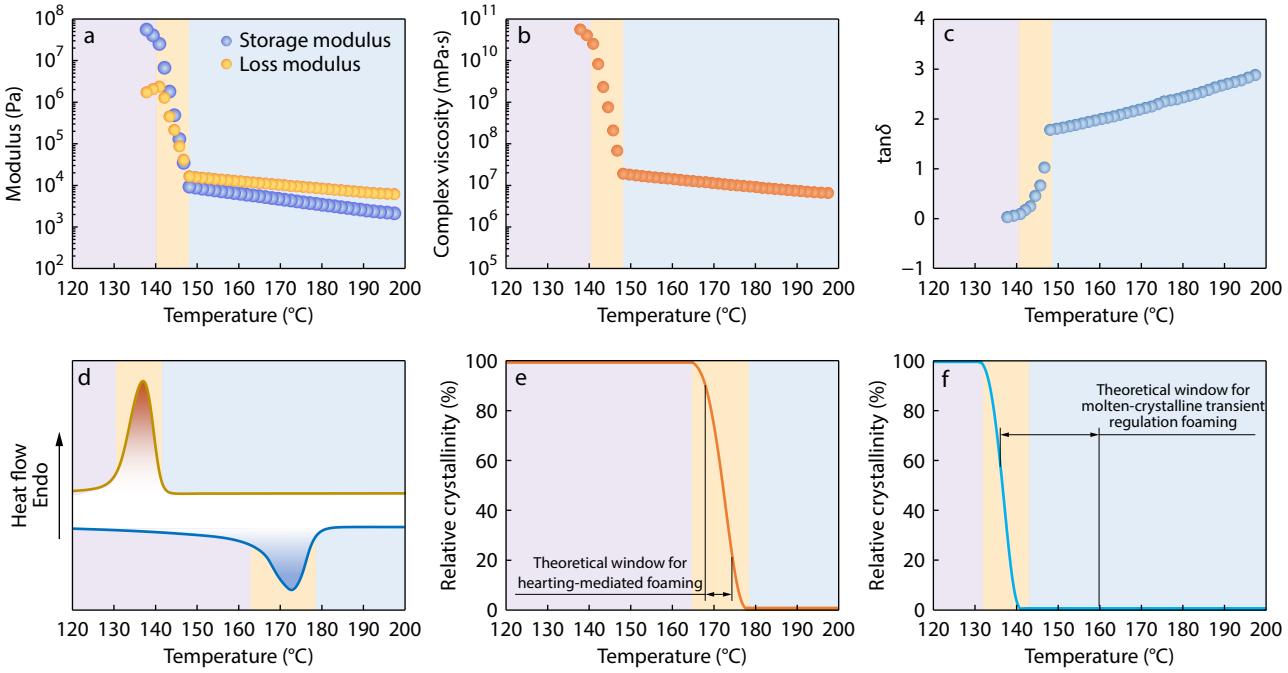

Fig. 2 Rheological and thermal characterization of PVDF. (a) Temperature dependence of the storage modulus (G') and loss modulus (G''); (b) Temperature dependence of the complex viscosity (η^*); (c) Temperature dependence of the loss tangent (tanδ); (d) DSC thermograms obtained during heating and cooling cycles. Evolution of the relative crystallinity of PVDF as a function of temperature during (e) heating and (f) cooling.

https://doi.org/10.1007/s10118-026-3803-6

sient regulation strategy, the sample prior to foaming exists as a homogeneous amorphous melt, as illustrated in Fig. 2(f). The melt strength gradually increased with decreasing temperature, and remained controllable before the onset of crystallization. This enabled stable cell growth and fixation within the uniform melt, making both the expansion ratio and cell morphology easier to control. Once the temperature drops below the onset of crystallization, rapid crystal formation occurs, which effectively restricts further cell growth. Consequently, in this strategy, the lower bound of the foaming window is determined by the crystallization onset temperature, whereas the upper bound is governed by the melt strength, resulting in an overall wider processing window. In summary, owing to its suitable melt strength prior to crystallization, PVDF exhibits a broader foaming window under the molten-crystalline transient regulation strategy, enabling a more complete realization of its foaming potential.

Foaming Performance

Fig. 3 presents the representative SEM images of the PVDF foams. Within the temperature range of 120–160 °C, the foams exhibited a relatively uniform cellular structure, which is beneficial for achieving stable mechanical properties and broadening their potential applications. These results demonstrate the excellent applicability of the molten-crystalline transient regulation foaming strategy, effectively widening the processing window for semi-crystalline polymers.

Fig. 4(a) shows the expansion ratio of the PVDF foams as a function of foaming temperature. Compared with the conventional heating-mediated process, the foaming temperature window was significantly expanded, underscoring the superior foamability and processing stability of the molten-crystalline transient regulation strategy. A maximum expansion ratio of 33.4 was achieved at 13.8 MPa and 140 °C. As the saturation pressure increased from 13.8 MPa to 27.6 MPa, the maximum expansion ratio at each pressure gradually decreased to 28.3, and the optimal foaming temperature shifted from 140 °C to 135 °C. The higher CO_2 solubility at elevated pressures enhances the plasticizing effect and foaming driving force. Consequently, a higher melt strength is required to facilitate sufficient cell growth, which explains the decrease in the optimal foaming temperature. Polymer foams with expansion ratios exceeding 5 exhibit good characteristics of light weight and well-defined cell morphology. To better quantify the foamability of PVDF under the molten-crystalline transient regulation strategy, the foaming temperature window was defined as the temperature range over which the expansion ratio exceeded 5. The bell-shaped curves of temperature versus expansion ratio in Fig. 4(a) indicate that the foaming temperature windows of PVDF foams can be determined as 120–160 °C under three different saturation pressures.

Figs. 4(b) and 4(c) further display the variations in cell density and cell size with foaming temperature under different saturation pressures. Increasing the saturation pressure markedly increased the cell density while reducing the cell size. In contrast, the influence of foaming temperature on the cellular structure was less pronounced. Generally, both cell density and cell size initially increased and then decreased with rising foaming temperature. This trend can be attributed to the high resistance to cell growth caused by excessive melt strength at lower temperatures, and the limited ability of the polymer matrix to retain dissolved gas due to insufficient melt strength at higher temperatures.[42]

Notably, well-defined open-cell structures were observed under appropriate foaming conditions, as illustrated in the red box insets of Fig. 3. A quantitative analysis of the open-cell content under different foaming conditions is shown in Fig. 4(d). By adjusting the processing parameters, PVDF foam with an open-cell content as high as 94.7% was obtained. The open-cell structure was typically formed at appropriate foaming temperatures. Under these conditions, the PVDF melt contained almost no crystals, and its melt strength was sufficient to enable relatively uniform stretching of the cell walls during growth, thereby ensuring a high expansion ratio. As the cell walls thinned during expansion, their surface tension increased, and their strength decreased, making them prone to rupture under biaxial stress.[43] Simultaneously, strain-induced crystallization occurred in the molecular chains. The

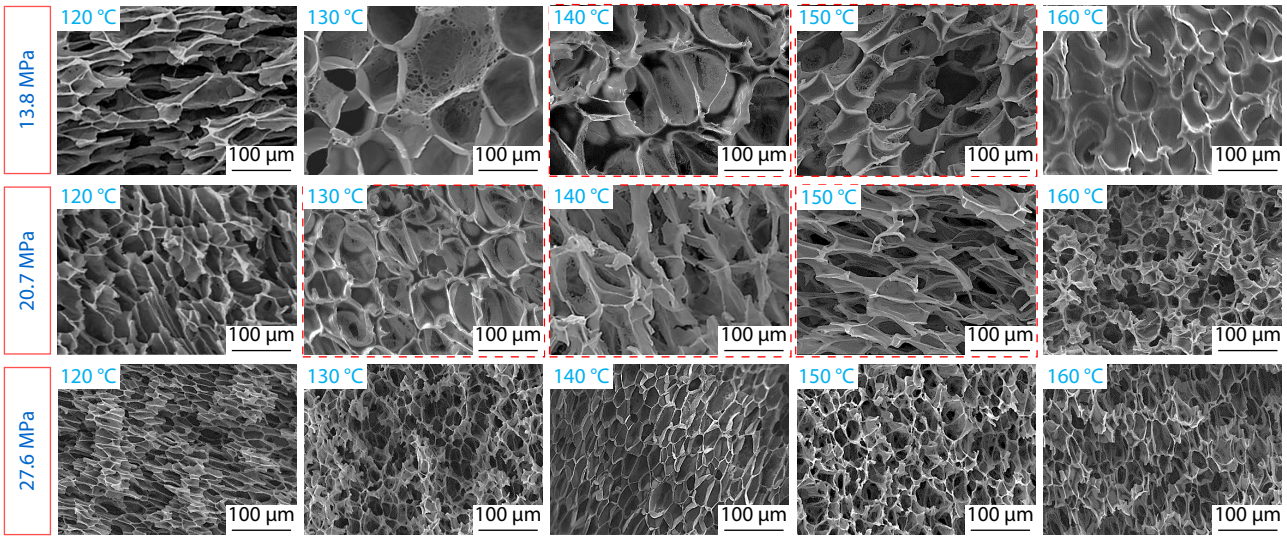

Fig. 3 Representative SEM images of the cellular morphologies of PVDF foams prepared under different foaming conditions.

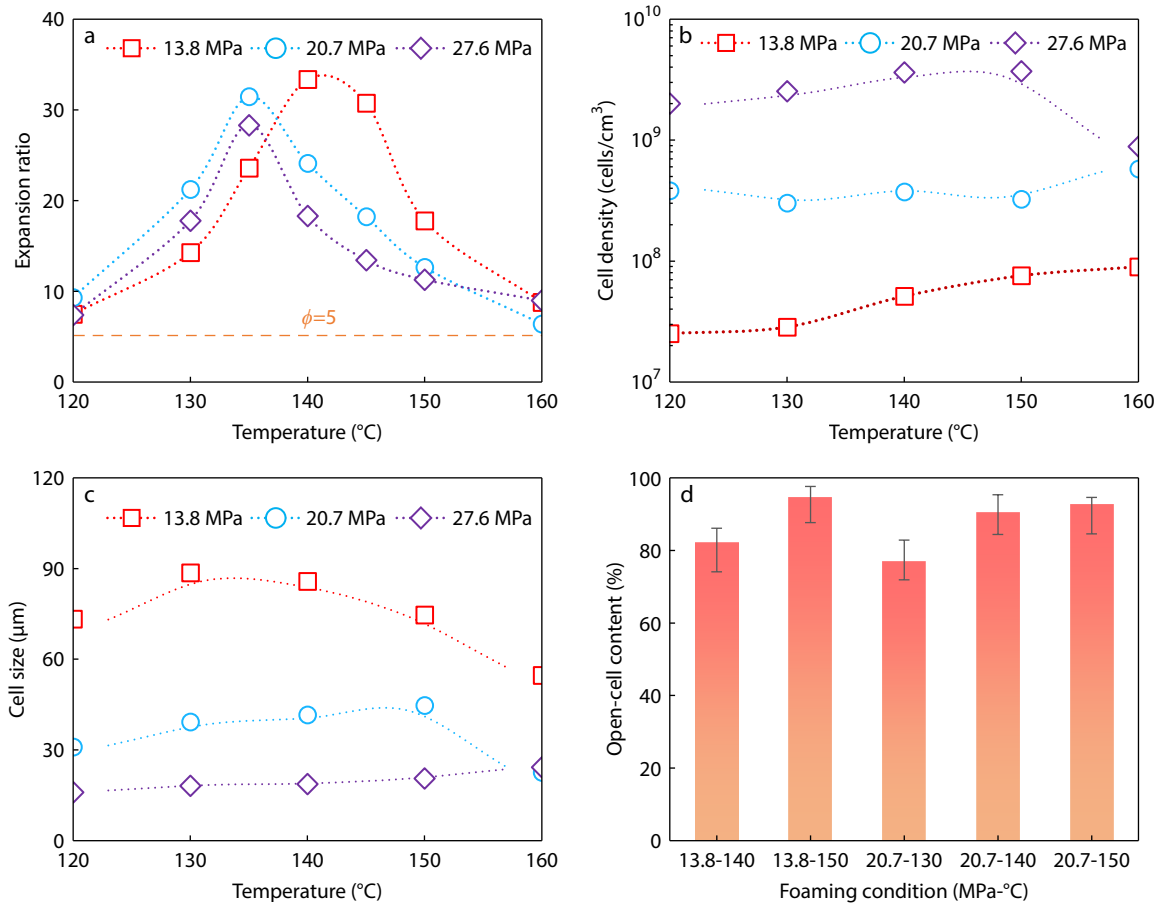

Fig. 4 Foaming performance of PVDF under various saturation pressures. (a) Expansion ratio, (b) cell density, and (c) cell size as functions of foaming temperature at saturation pressures of 13.8, 20.7, and 27.6 MPa. (d) Open porosity of the resulting PVDF foams prepared across the corresponding temperature and pressure conditions.

matrix shrinkage caused by the closely packed crystalline regions, coupled with the modulus mismatch between the crystalline and amorphous phases in the cell walls, led to stress concentration at the weak points, thereby inducing the formation of open-cell structures.[7] Consequently, the molten-crystalline transient regulation strategy facilitated the development of highly interconnected open-cell structures at elevated temperatures.

In microcellular foaming, the foamability of a polymer is primarily governed by its melt strength, and the melt strength of PVDF is strongly influenced by its crystallization behavior. Numerous studies have demonstrated that in heating-mediated foaming processes, the remaining lamellae may maintain relatively strong inter-lamellar interactions, which can impose considerable resistance to cell growth.[44,45] Once the temperature exceeds the melting point, the crystals melt rapidly within an extremely narrow temperature range, as illustrated in Fig. 5. This rapid melting is generally triggered by the combined effects of heat and $scCO_2$, which induces a sudden increase in the mobility of flexible molecular chains. Consequently, the melt strength of PVDF undergoes an abrupt transition from excessively high to excessively low, resulting in an extremely narrow foaming window of 157–162 °C. This significantly increases the difficulty of controlling the foaming conditions and limits the achievable expansion ratio.

In the microcellular foaming process employing the molten-crystalline transient regulation strategy, the crystals are first completely melted at a higher temperature. During the subsequent cooling process, the plasticization effect of $scCO_2$ enhances the mobility of PVDF molecular chains, allowing chain arrangement and crystallization to proceed over a broader temperature range, approximately from 190 °C to 120 °C. Therefore, the presence of CO_2 is proposed to promote the gradual formation of crystals within this temperature range, thereby helping to establish a suitable crystalline network and melt strength for cell growth. Furthermore, as shown in the SEM images in Fig. 3, when the foaming temperature was further decreased to 120 °C, the cells exhibited an unconventional polygonal or hexagonal morphology. This phenomenon suggests that, at this lower foaming temperature, the amount of crystals present in the melt may have increased beyond a certain threshold. These crystals can restrict the deformation and expansion of the surrounding polymer matrix, thereby compressing the growing cells and affecting the final cell morphology. In conclusion, the molten-crystalline transient regulation strategy can exploit the foamability of PVDF more simply and effectively. Benefiting from this mechanism, the foaming temperature window of PVDF foam in this study expands to 120–160 °C, representing a 567% increase compared to the heating-mediated process.[45]

https://doi.org/10.1007/s10118-026-3803-6

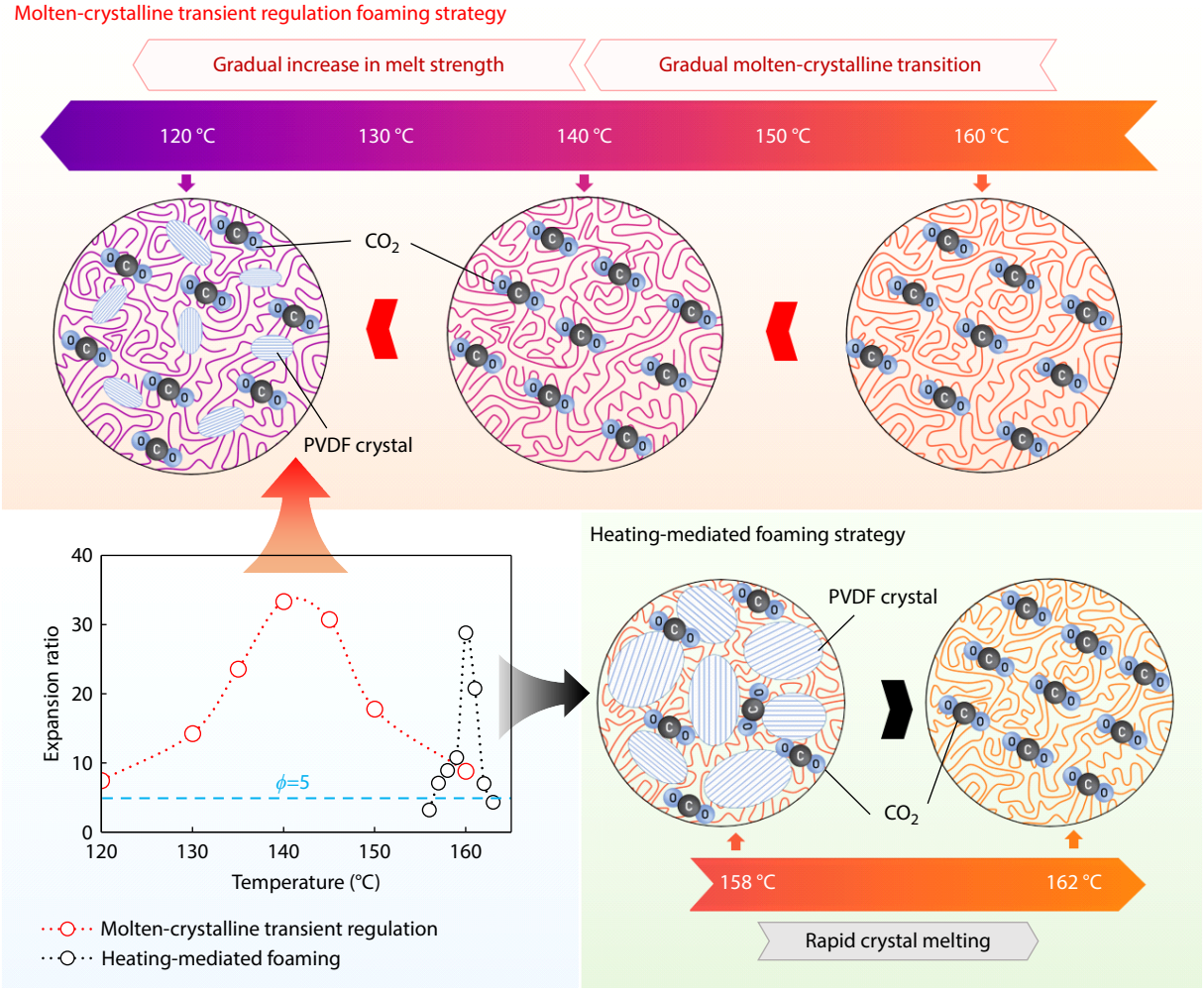

Fig. 5 Schematic diagram comparing the molten-crystalline transient regulation foaming strategy with the conventional heating-mediated foaming strategy.

Meanwhile, the maximum expansion ratio increases from 28.8 to 33.4, equivalent to a 16.0% improvement.

Oil Adsorption Performance

Open-cell microcellular polymer foams are promising sorbents for waste oil treatment. Fig. 6(a) shows a representative SEM image of the PVDF foam, revealing a well-developed open-cell architecture with an open-cell content of 94.7%. Such a highly interconnected structure, together with a large specific surface area and a high expansion ratio, is expected to facilitate rapid oil uptake and a high sorption capacity. To demonstrate practical oil–water separation, Fig. 6(b) presents a simulated cleanup process using PVDF foam. Both ethyl acetate floating on the water surface and carbon tetrachloride (CCl_4) submerged in water were rapidly and completely removed by the foam. The distinct wetting behavior toward water and oil is further illustrated in Fig. 6(c), where the water droplets and CCl_4 were colored with methylene blue and Sudan III, respectively. The water droplet maintained a nearly spherical shape on the foam surface, exhibiting a high water contact angle of 127°, whereas CCl_4 spread readily and penetrated into the porous network. These observations confirm the pronounced hydrophobicity and oleophilicity of the PVDF foam and indicate that the foam surface provides uniform and effective oil uptake, highlighting its potential for waste oil recovery and water purification.[46]

Figs. 6(d) and 6(f) compare the time-dependent sorption capacities of the PVDF foam for various oils with different viscosities. Low-viscosity oils (CCl_4, ethyl acetate, diesel and cyclohexane) and high-viscosity oils (peanut oil and silicone oil) were selected to elucidate the viscosity effect on uptake behavior. Among the low-viscosity oils, the foam exhibits the highest sorption capacity toward CCl_4 (about 28.0 $g \cdot g^{-1}$), followed by ethyl acetate (about 16.7 $g \cdot g^{-1}$), diesel (about 14.8 $g \cdot g^{-1}$), and cyclohexane (about 13.7 $g \cdot g^{-1}$). For high-viscosity oils, the capacity for silicone oil (about 18.2 $g \cdot g^{-1}$) is higher than that for peanut oil (about 15.7 $g \cdot g^{-1}$). For all oils, the sorption capacity increases rapidly at the initial stage and then approaches equilibrium. Notably, low-viscosity oils reach equilibrium within 7 min, whereas high-viscosity oils require about 45 min, which can be attributed to the larger diffusion resistance and slower transport kinetics in viscous liquids. The sorption kinetics can be described by the pseudo-second-order model:[7]

$$\frac{t}{Q_t} = \frac{t}{Q_e} + \frac{1}{kQ_e^2} \quad (5)$$

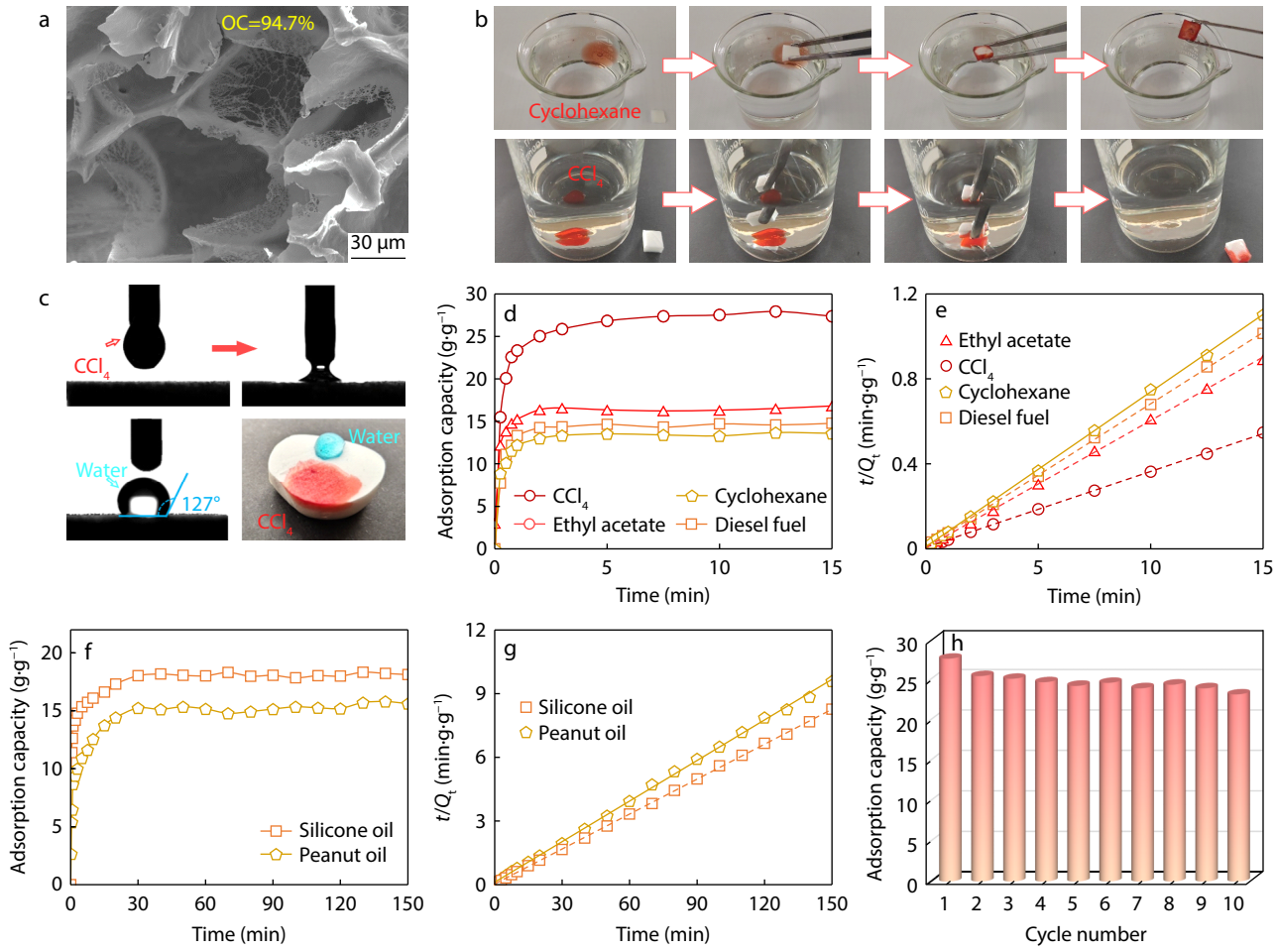

Fig. 6 Characterization of the PVDF open-cell foam for oil/water separation. (a) Representative SEM image showing its cellular morphology; (b) Schematic of the adsorption process for cyclohexane and CCl_4; (c) Contact angle measurement and comparative wetting behavior of a water droplet versus dyed CCl_4 on the foam surface; (d) Adsorption capacity and (e) corresponding kinetic plot (t/Q_t) for a low-viscosity oil; (f) Adsorption capacity and (g) kinetic plot (t/Q_t) for a high-viscosity oil; (h) Adsorption capacity for CCl_4 over 10 consecutive adsorption–recovery cycles, demonstrating reusability.

where Q_t is the sorption capacity at time t, Q_e is the equilibrium sorption capacity, and k is the rate constant. As shown in Figs. 6(e) and 6(g), a good linear relationship between t/Q_t and t was obtained, indicating that the model adequately captured the sorption behavior. The fitted parameters are listed in Table 1. The rate constants for CCl_4, ethyl acetate, diesel, and cyclohexane were 2.91×10^{-3}, 9.77×10^{-3}, 7.47×10^{-3}, and 9.25×10^{-3} $g\cdot g^{-1}\cdot s^{-1}$, respectively, which were substantially higher than those for silicone oil and peanut oil (1.32×10^{-3} and 0.58×10^{-3} $g\cdot g^{-1}\cdot s^{-1}$). This further confirms the faster uptake kinetics of low-viscosity oils and demonstrates the efficient oil-sorption performance of the open-cell PVDF foam.

Table 1 Fitting parameters of PVDF foam based on pseudo-second-order kinetic model.

	Q_e ($g\cdot g^{-1}$)	k ($g\cdot g^{-1}\cdot s^{-1}$)	R^2
CCl_4	28.0	2.91×10^{-3}	0.9998
Ethyl acetate	16.7	9.77×10^{-3}	0.9997
Diesel fuel	14.8	7.47×10^{-3}	0.9998
Cyclohexane	13.7	9.25×10^{-3}	0.9998
Silicone oil	18.2	1.32×10^{-3}	0.9998
Peanut oil	15.7	0.58×10^{-3}	0.9994

Reusability is critical for practical oil-spill cleanup because it improves operational efficiency and reduces treatment costs. Therefore, the cyclic sorption performance and compressive recovery of the PVDF foam were evaluated. Fig. 6(h) shows the sorption capacity of CCl_4 over repeated cycles. The capacity decreased gradually during the first five cycles and stabilized thereafter. After 10 adsorption–desorption cycles, the sorption capacity decreased by 16%, but remained above 23 $g\cdot g^{-1}$, indicating good recyclability for repeated oil recovery.

Compression and Thermally Insulation of PVDF Foams

Compressive resistance is a key performance metric of microcellular polymer foams. Fig. 7(a) shows the compressive stress-strain curves of the PVDF foams with a comparable cell size (approximately 46 μm) but different expansion ratios. All curves exhibit the three characteristic deformation regimes of cellular solids: first, a linear elastic region, where stress increases approximately linearly with strain; second, a plateau region associated with progressive cell wall and strut buckling and collapse,

https://doi.org/10.1007/s10118-026-3803-6

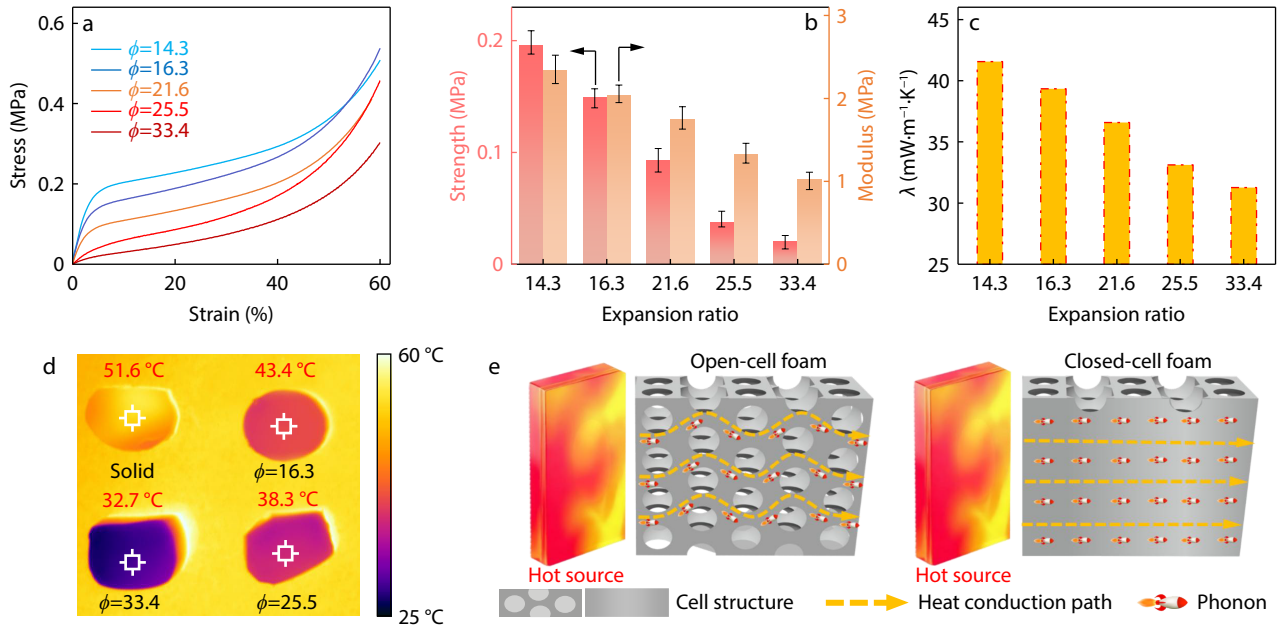

Fig. 7 Mechanical and thermal properties of PVDF foams with varied expansion ratios. (a) Compressive stress-strain curves; (b) Corresponding compressive strength and modulus; (c) Thermal conductivity as a function of expansion ratio; (d) Infrared thermal images comparing the surface temperatures of solid PVDF and foam samples placed on an 80 °C hot plate; (e) Schematic illustrating heat transfer within the open-cell and closed-cell foam structure.

during which the stress remains nearly constant; and third, a densification region, where stress rises sharply as collapsed cell walls come into contact and the solid matrix dominates the deformation. The compressive modulus was determined from the slope of the initial linear elastic region, whereas the compressive strength was typically taken as the stress level at the onset of the plateau (or the stress at a specified strain, depending on the adopted standard). As summarized in Fig. 7(b), increasing the expansion ratio from 14.3 to 33.4 leads to a pronounced reduction in compressive performance: the compressive strength decreases from 0.20 MPa to 0.02 MPa, and the compressive modulus decreases from 2.34 MPa to 1.02 MPa. This trend is consistent with the Gibson-Ashby model for cellular solids:[47]

$$\sigma_{pl} \approx \sigma_{ys}\left[0.3\left(\frac{\zeta}{\varphi}\right)^{3/2} + 0.4\frac{(1-\zeta)}{\varphi}\right] \quad (6)$$

where σ_{pl} is the compressive strength of the foam, σ_{ys} is the yield strength of solid PVDF, ζ and $(1-\zeta)$ represent the volume fractions associated with cell struts and cell walls, respectively. A higher expansion ratio corresponded to a lower relative density. The reduced volume fraction of the load-bearing solid phase leads to diminished strength and stiffness.

The thermal conductivities of samples with different expansion ratios were measured to evaluate the thermal insulation performance of the open-cell PVDF foams. As shown in Fig. 7(c), quantitative measurements reveal that the thermal conductivity decreases from 41.56 $mW{\cdot}m^{-1}{\cdot}K^{-1}$ to 31.26 $mW{\cdot}m^{-1}{\cdot}K^{-1}$ as the expansion ratio increases from 14.3 to 33.4. In Fig. 7(d), infrared thermography was used to monitor the surface temperature of PVDF specimens placed on an 80 °C hot stage, simulating their effectiveness in practical application scenarios. As the expansion ratio increased from 16.3 to 33.4, the surface temperature decreased from 43.4 °C to 32.7 °C. Compared to the surface temperature of solid PVDF (51.6 °C), the PVDF foams with higher expansion ratios exhibited improved thermal insulation. This behavior can be rationalized using the heat-transfer model for microcellular foams:[48]

$$\lambda = (1-\varepsilon)\,\xi\lambda_{sol} + \varepsilon\lambda_{gas} + \lambda_{rad} \quad (7)$$

where ε is the gas volume fraction, ξ is a tortuosity factor reflecting the structural complexity of the foam, and λ_{sol}, λ_{gas} and λ_{rad} the contributions from the solid phase, gas phase, and thermal radiation, respectively. Increasing the expansion ratio reduced the fraction of the high-thermal-conductivity solid phase per unit volume, thereby lowering the overall thermal conductivity. Moreover, as schematically illustrated in Fig. 7(e), the porous features on the cell walls increased the effective heat-transfer path length and intensified phonon scattering, which further suppressed the heat transport and enhanced the energy dissipation.[27] Consequently, open-cell PVDF foams exhibit excellent thermal insulation performance.

Table 2 presents representative parameters of the oil adsorption and thermal insulation performance of the PVDF foam prepared in this work and other open-cell materials reported in the literature. It can be seen that, compared with other porous materials, the PVDF foam prepared herein exhibits a considerably large or even larger adsorption capacity and better thermal insulation performance. The $scCO_2$ foaming technology employed in this work offers the advantages of being environmentally friendly and efficient, which is more conducive to green production than other materials prepared using chemical technology. Therefore, the PVDF open-cell foam fabricated based on the molten-crystalline transient regulation strategy is an ideal material for addressing oil pollution and improving thermal management efficiency.

https://doi.org/10.1007/s10118-026-3803-6

Table 2 Comparison of representative properties between PVDF foam prepared in this work and porous materials reported in other literature.

Material	Expansion ratio	Open-cell content (%)	Oil adsorption capacity ($g \cdot g^{-1}$)	Type of oils	Thermal conductivity ($mW \cdot m^{-1} \cdot K^{-1}$)	Ref.
EG-PVDF foam	11.5	–	4.1–7.0	Chloroform, soybean oil, *n*-heptane, *etc.*	–	[49]
PVDF/EG foam	9	–	12	Soybeans oil	–	[50]
PVDF aerogel	–	–	3.10–6.78	Hexane, toluene, dichloromethane, *etc.*	–	[51]
PLA foam	39.2	–	4.6–15.1	CCl_4, ethyl acetate, *n*-octane, thermal oil	–	[52]
PLA/TPU foam	36.0	96.2	4.7–18.8	CCl_4, cyclohexane, diesel oil, silicone oil	–	[17]
PLA/PMMA foam	44	93.1	10.1–30.9	Cyclohexane, diesel, CCl_4, *etc.*	31.7	[28]
UHMWPE/HDPE foam	36.5	–	10–15	CCl_4, cyclohexane	39.81	[53]
UHMWPE/GNPs foam	35.9	–	30–50.6	CCl_4, gasoline, cyclohexane	36.9	[54]
PVDF foam	33.4	94.7	13.7–28.0	CCl_4, ethyl acetate, silicone oil, *etc.*	31.26	This work

CONCLUSIONS

Highly expanded open-cell PVDF foams with excellent oil adsorption and thermal-insulation performance were fabricated *via* a molten-crystalline transient regulation strategy in microcellular foaming with $scCO_2$. During the foaming process, the plasticizing effect of $scCO_2$ postponed the undercooling-induced crystallization of PVDF to a lower temperature, resulting in a more gradual evolution of the melt strength over a wider temperature range, thereby enabling easier regulation of the melt strength. By adjusting the foaming parameters, PVDF exhibited good foaming performance within a broad processing window of 120–160 °C and 13.8–21.7 MPa, achieving an expansion ratio as high as 33.4. The absence of crystal reinforcement in the melt during foaming, combined with uniform thinning of the cell walls under biaxial stretching, along with modulus mismatch between the strain-induced crystalline regions and the amorphous domains, leading to localized stress concentration, promoted cell wall rupture and thus enabled the construction of an interconnected structure with an open-cell content up to 94.7%. Benefiting from its high open-cell content and expansion ratio, the PVDF foam exhibited pronounced hydrophobicity and oleophilicity, allowing it to efficiently remove waste oil from water. Its oil adsorption capacity for various oils reached 13.7–28.0 $g \cdot g^{-1}$, with adsorption rate constants ranging from 0.58×10^{-3} $g \cdot g^{-1} \cdot s^{-1}$ to 9.77×10^{-3} $g \cdot g^{-1} \cdot s^{-1}$, and it demonstrated good reusability. The foam also showed tunable compressive properties: as the expansion ratio increased from 14.3 to 33.4, the compressive strength decreased from 0.20 MPa to 0.02 MPa, and the compressive modulus decreased from 2.34 MPa to 1.02 MPa. Furthermore, the open-cell PVDF foam exhibited excellent thermal insulation performance, with a thermal conductivity as low as 31.26 $mW \cdot m^{-1} \cdot K^{-1}$, which is attributed to the microporous features of the cell walls that hinder heat transfer. Combined with the inherent chemical resistance and weatherability of the PVDF matrix, these highly open-cell PVDF foams are expected to serve as efficient, safe, and sustainable materials for oil purification and thermal insulation for future applications.

Conflict of Interests

The authors declare no interest conflict.

Data Availability Statement

The data that support the findings of this study are available from the corresponding author upon reasonable request.

ACKNOWLEDGMENTS

This work was financially supported by the National Natural Science Foundation of China (Nos. 52675467 and 52605568), Shandong Provincial Key Research and Development Program (Results to Market) (No. 2026CGZSC0114), Matching Support Program for National Leading Talents in Shandong Province (No. 2022GJJLJRC-01), Funding Project of Jinan City's New Twenty Items for Colleges and Universities (No. 202333038), and Shandong University Distinguished Professor Program.

REFERENCES

1 Omer, A. M. Energy, environment and sustainable development. *Renew. Sust. Energ. Rev.* **2008**, *12*, 2265–2300.
2 Tan, H.; Li, J.; He, M.; Li, J.; Zhi, D.; Qin, F.; Zhang, C. Global evolution of research on green energy and environmental technologies: a bibliometric study. *J. Environ. Manage.* **2021**, *297*, 113382.
3 Radu, I. C.; Vadureanu, A. M.; Cozorici, D. E.; Blanzeanu, E.; Zaharia, C. Advancing sustainability in modern polymer processing: strategies for waste resource recovery and circular economy integration. *Polymers* **2025**, *17*, 522.
4 Hohne, P. A.; Kusakana, K.; Numbi, B. P. Improving energy efficiency of thermal processes in healthcare institutions: a review on the latest sustainable energy management strategies. *Energies* **2020**, *13*, 569.
5 Mansour, M. S.; Abdel-Shafy, H. I.; Ibrahim, A. M. Petroleum wastewater: Environmental protection, treatment, and safe reuse: an overview. *J. Environ. Manage.* **2024**, *351*, 119827.
6 Zafirakou, A.; Themeli, S.; Tsami, E.; Aretoulis, G. Multi-criteria analysis of different approaches to protect the marine and coastal environment from oil spills. *J. Mar. Sci. Eng.* **2018**, *6*, 125.
7 Li, B.; Zhao G.; Wang G.; Zhang L.; Gong J.; Shi Z. Biodegradable PLA/PBS open-cell foam fabricated by supercritical CO_2 foaming for selective oil-adsorption. *Sep. Purif. Technol.* **2021**, *257*, 117949.
8 Bing, X.; Ma, W.; Wu, M.; Gao, P.; Zhou, X.; Luo, H.; Wang, L.; Zheng, W. Lightweight, strong and high heat-resistant poly(lactide acid) foams *via* microcellular injection molding with self-assembly nucleating agent. *Chinese J. Polym. Sci.* **2024**, *42*, 739–750.
9 Jiang, J. P.; Deng, S. D.; Lee, S. H.; Lum, W. C.; Ren, Y. H.; Du, G. B.; Zhou. X. J.; Zhang, J. Characterization of biodegradable flame retardant rigid polyurethane foam prepared using renewable epoxidized soybean oil and ricinoleic acid. *Chinese J. Polym. Sci.* **2025**, *43*, 1346–1366.

Graphical Abstract

Highly Expanded Open-cell Poly(vinylidene fluoride) Foams Achieved by Microcellular Foaming for Efficient Oil Adsorption and Thermal Insulation

Chao Wei, Jia-Long Chai, Lei Zhang, Zhao-Rui Xu, and Gui-Long Wang

Shandong University; Linyi Huafeng Seal Technology Co., Ltd.

The molten-crystalline transient regulation strategy in microcellular foaming effectively controls crystallization behavior for suitable melt structure and strength, producing highly expanded open-cell poly(vinylidene fluoride) (PVDF) foams with promising potential for oil adsorption and thermal insulation.

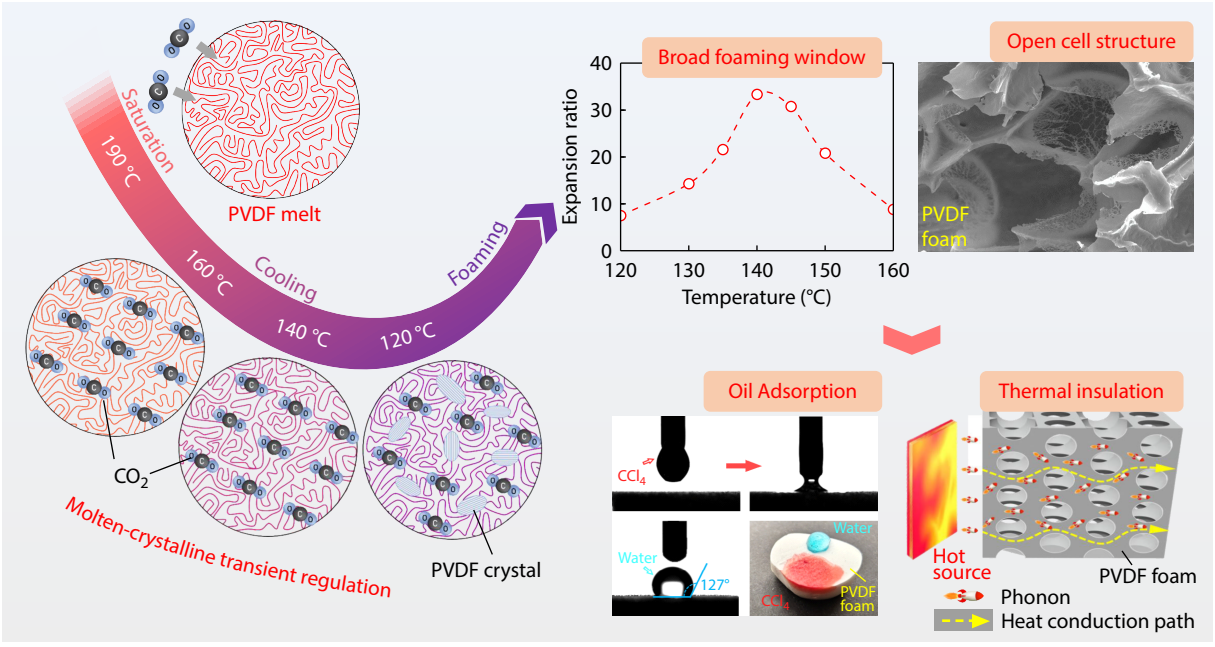

Chinese J. Polym. Sci. 2026 *https://doi.org/10.1007/s10118-026-3803-6*

10 Li, Y.; Shen, B.; Yi, D.; Zhang, L.; Zhai, W.; Wei, X.; Zheng, W. The influence of gradient and sandwich configurations on the electromagnetic interference shielding performance of multilayered thermoplastic polyurethane/graphene composite foams. *Compos. Sci. Technol.* **2017**, *138*, 209–216.
11 Wang, Y.; Yang, H.; Chen, Z.; Chen, N.; Pang, X.; Zhang, L.; Minari, T.; Liu X.; Liu, H.; Chen, J. Recyclable oil-absorption foams *via* secondary phase separation. *ACS Sustainable Chem. Eng.* **2018**, *6*, 13834–13843.
12 Gui, H.; Zhang, T.; Guo, Q. Nanofibrous, emulsion-templated syndiotactic polystyrenes with superhydrophobicity for oil spill cleanup. *ACS Appl. Mater. Interfaces* **2019**, *11*, 36063–36072.
13 Gwon, J. G.; Kim, S. K.; Kim, J. H. Sound absorption behavior of flexible polyurethane foams with distinct cellular structures. *Mater. Design* **2016**, *89*, 448–454.
14 Kamińska, K.; Barczewski, M.; Kurańska, M.; Malewska, E.; Polaczek, K.; Prociak, A. The effect of a chemical foaming agent and the isocyanate index on the properties of open-cell polyurethane foams. *Materials* **2022**, *15*, 6087.
15 Chollon, G.; Delettrez, S.; Langlais, F. Chemical vapour infiltration and mechanical properties of carbon open-cell foams. *Carbon* **2014**, *66*, 18–30.
16 Zhao, J.; Huang, Y.; Wang, G.; Qiao, Y.; Chen, Z.; Zhang, A.; Park, C. B. Fabrication of outstanding thermal-insulating, mechanical robust and superhydrophobic PP/CNT/sorbitol derivative nanocomposite foams for efficient oil/water separation. *J. Hazard. Mater.* **2021**, *418*, 126295.
17 Cui, S.; Wu, M.; Xu, M.; Li, X.; Ren, Q.; Wang, L.; Zheng, W. Supercritical CO_2 extrusion foaming of highly open-cell poly (lactic acid) foam with superior oil adsorption performance. *Int. J. Biol. Macromol.* **2024**, *269*, 132138.
18 Li, Z.; Jiang, J.; Qiao, M.; Xie, Y.; Zhang, Y.; Zhu, C.; Wang X.; Li, Q. Biodegradable ultra-large expansion and high open-cell PLA/PBAT foams fabricated by supercritical CO_2 foaming for selective oil/water absorption. *J. Polym. Environ.* **2024**, *32*, 4647–4660.
19 Lima, G. M.; Bose, R. K. Production and application of polymer foams employing supercritical carbon dioxide. *Adv. Polym. Technol.* **2022**, *1*, 8905115.
20 Jiang, J.; Yang, S.; Qiao, M.; Li, Z.; Wang, X.; Zhu, C.; Li, Q. Achieving lightweight, low-shrinkage and superior elastic poly(butylene adipate-co-terephthalate) open-cell foams *via*

ultrasonic-enhanced microcellular foaming. *J. Polym. Environ.* **2025**, *33*, 4906–4920.
21 Rodeheaver, B. A.; Colton, J. S. Open-celled microcellular thermoplastic foam. *Polym. Eng. Sci.* **2001**, *41*, 380–400.
22 Li, D.; Zhang, S.; Zhao, Z.; Miao, Z.; Zhang, G.; Shi, X. High-expansion open-cell polylactide foams prepared by microcellular foaming based on stereocomplexation mechanism with outstanding oil–water separation. *Polymers* **2023**, *15*, 1984.
23 Yu, P.; Mi, H.; Huang, A.; Geng, L.; Chen, B.; Kuang, T.; Mou, W.; Peng, X. Effect of poly (butylenes succinate) on poly (lactic acid) foaming behavior: formation of open cell structure. *Ind. Eng. Chem. Res.* **2015**, *54*, 6199–6207.
24 Nivedhitha, D. M.; Jeyanthi, S. Polyvinylidene fluoride, an advanced futuristic smart polymer material: a comprehensive review. *Polym. Adv. Technol.* **2023**, *34*, 474–505.
25 Concha, V. O.; Timóteo, L.; Duarte, L. A.; Bahú, J. O.; Munoz, F. L.; Silva, A. P.; Souto, E. B. Properties, characterization and biomedical applications of polyvinylidene fluoride (PVDF): a review. *J. Mater. Sci.* **2024**, *59*, 14185–14204.
26 Pan, Y.; Zhu, Z.; Li, M.; Cheng, C.; Wang, M.; Jiao, R.; Sun H.; Li, A. Preparation of halloysite-based PVDF membrane for effective oil/water separation and dyes removal. *Sep. Purif. Technol.* **2025**, *359*, 130595.
27 Shi, Z.; Zhao, G.; Zhang, L.; Wang, G.; Chai, J. Ultralight and hydrophobic PVDF/PMMA open-cell foams with outstanding heat-insulation and oil-adsorption performances fabricated by CO_2 molten foaming. *J. CO_2 Util.* **2022**, *63*, 102108.
28 Dallaev, R.; Pisarenko, T.; Sobola, D.; Orudzhev, F.; Ramazanov, S.; Trčka, T. Brief review of PVDF properties and applications potential. *Polymers-Basel* **2022**, *14*, 4793.
29 Mancarella, C.; Martuscelli, E. Crystallization kinetics of poly(vinylidene fluoride). *Polymer* **1977**, *18*, 1240–1242.
30 Gradys, A.; Sajkiewicz, P.; Zhuravlev, E.; Schick, C. Kinetics of isothermal and non-isothermal crystallization of poly(vinylidene fluoride) by fast scanning calorimetry. *Polymer* **2016**, *82*, 40–48.
31 Mohebbi, A.; Mighri, F.; Ajji, A.; Rodrigue, D. Current issues and challenges in polypropylene foaming: a review. *Cell. Polym.* **2015**, *34*, 299–338.
32 Jiang, J.; Tian, F.; Li, Y.; Qin, Z.; Huang, H.; Zhai, W. The critical role of crystalline state in dictating the foaming window and morphology of homopolymer versus copolymer polypropylene. *Polymer* **2025**, *343*, 129408.
33 Fu, L.; Shi, Q.; Ji, Y.; Wang, G.; Zhang, X.; Chen, J.; Shen C.; Park, C. B. Improved cell nucleating effect of partially melted crystal structure to enhance the microcellular foaming and impact properties of isotactic polypropylene. *J. Supercrit. Fluid.* **2020**, *160*, 104794.
34 Li, B.; Zhao, G.; Wang, G.; Zhang, L.; Gong, J. Fabrication of high-expansion microcellular PLA foams based on pre-isothermal cold crystallization and supercritical CO_2 foaming. *Polym. Degrad. Stabil.* **2018**, *156*, 75–88.
35 Wang, Z.; Wang, B.; Wang, Y.; Bian, J.; Hua, Y.; Li, Q.; Cai, W. Mechanism of CO_2 dissolution and crystallization influenced by temperature in the condensation of high-CO_2 natural gas: A molecular dynamics study. *Int. J. Heat Mass Tran.* **2025**, *253*, 127521.
36 Zhang, L.; Zhao, G.; Wang, G. Investigation on the growth of snowflake-shaped Poly (L-Lactic acid) crystal by in-situ high-pressure microscope. *Polymer* **2019**, *177*, 25–34.
37 Zheng, Y.; Zhang, C.; Bao, Y.; Shan, G.; Pan, P. Temperature-dependent crystallization and phase transition of poly (L-lactic acid)/CO_2 complex crystals. *Chinese J. Polym. Sci.* **2021**, *39*, 484–492.
38 Chai, J.; Wang, G.; Wei, C.; Li, X.; Shao, R.; Zhao, G. Ultra-expanded microcellular shape memory polymer foams *via* supercritical foaming for recyclable oil absorption and improved thermal insulation. *Adv. Ind. Eng. Polym. Res.* **2025**, *8*, 600–611.
39 Yu, K.; Wu, Y.; Zhang, X.; Hou, J.; Chen, J. Microcellular open-cell poly(l-lactic acid)/poly(d-lactic acid) foams for oil-water separation prepared *via* supercritical CO_2 foaming. *J. CO_2 Util.* **2022**, *65*, 102219.
40 Guo, H.; Jiang, J.; Li, Z.; Jin, Z.; Hou, J.; Wang, X.; Li, Q. Solid-state supercritical CO_2 foaming of PCL/PLGA blends: cell opening and compression behavior. *J. Polym. Environ.* **2020**, *28*, 1880–1892.
41 Li, J.; Wang, W.; Shi, Y.; Heck, B.; Luo, C.; de Claville Christiansen, J.; Yu D.; Reiter G.; Jiang, S. Crystallization and melting of polyethylene strongly cross-linked in the molten state. *Soft Matter* **2025**, *21*, 6422–6431.
42 Wang, G.; Wang, C.; Zhao, J.; Wang, G.; Park, C. B.; Zhao, G. Modelling of thermal transport through a nanocellular polymer foam: toward the generation of a new superinsulating material. *Nanoscale* **2017**, *9*, 5996–6009.
43 Mihai, M.; Huneault, M. A.; Favis, B. D.; Li, H. Extrusion foaming of semi-crystalline PLA and PLA/thermoplastic starch blends. *Macromol. Biosci.* **2007**, *7*, 907–920.
44 Zhao, B.; Zhao, C.; Wang, C.; Park, C. B. Poly(vinylidene fluoride) foams: a promising low-*k* dielectric and heat-insulating material. *J. Mater. Chem. C* **2018**, *6*, 3065–3073.
45 Wei, C.; Zhao, J.; Wang, G.; Chai, J.; Shi, Z.; Zhao, P.; Wang, Y. Strong and flame-retardant thermally insulating poly(vinylidene fluoride) foams fabricated by microcellular foaming. *Mater. Design* **2022**, *221*, 110932.
46 Chai, J.; Wang, G.; Zhang, A.; Zhao, G.; Park, C. B. Superhydrophobic nanofibrous polytetrafluoroethylene and composite membranes with tunable adhesion for micro-droplet manipulation, self-cleaning and oil/water separation. *J. Environ. Chem. Eng.* **2024**, *12*, 112355.
47 Zhao, J.; Zhao, Q.; Wang, L.; Wang, C.; Guo, B.; Park, C. B.; Wang, G. Development of high thermal insulation and compressive strength BPP foams using mold-opening foam injection molding with in-situ fibrillated PTFE fibers. *Eur. Polym. J.* **2018**, *98*, 1–10.
48 Wang, Z.; Wang, G.; Xu, Z.; Ma, C.; Zhao, G. Pore-gradient, flexible, and fully-degradable foam with outstanding noise absorption and thermal insulation. *Adv. Funct. Mater.* **2025**, *35*, 2504560.
49 Tian, Y.; Ma, H. Solvent-free green preparation of reusable EG-PVDF foam for efficient oil-water separation. *Sep. Purif. Technol.* **2020**, *253*, 117506.
50 Bentini, R.; Pola, A.; Rizzi, L. G.; Athanassiou, A.; Fragouli, D. A highly porous solvent free PVDF/expanded graphite foam for oil/water separation. *Chem. Eng. J.* **2019**, *372*, 1174–1182.
51 Chen, X.; Liang, Y.; Tang, X.; Shen, W.; Hu, X. Additive-free poly (vinylidene fluoride) aerogel for oil/water separation and rapid oil absorption. *Chem. Eng. J.* **2017**, *308*, 18–26.
52 Wang, S.; Yang, W.; Li, X.; Hu, Z.; Wang, B.; Li, M.; Dong, W. Preparation of high-expansion open-cell polylactic acid foam with superior oil-water separation performance. *Int. J. Biol. Macromol.* **2021**, *193*, 1059–1067.
53 Sun, X.; Wang, G.; Xu, Z.; Chai, J.; Zhang, A.; Zhao, G.; Li, S.; Wang, Y.; Jiao, H. Microcellular foaming-derived strong ultra-high molecular weight polyethylene/high-density polyethylene foams for thermally insulating and oil-water separating applications. *J. Environ. Chem. Eng.* **2024**, *12*, 113992.
54 Sun, X.; Wang, G.; Xu, Z.; Wang, Z.; Zhao, G. Advanced fabrication of ultra-high molecular weight polyethylene/graphite nanoplates foam for enhanced oil-water separation and thermal insulation *via* a novel omnidirectional gas escape barrier mechanism. *Chem. Eng. J.* **2025**, *503*, 158360.